Characterization of an IoT Stereo Image Sensor System for Weed Control

Bruno M. Moreno[1,2], Paulo E. Cruvinel[1,2]

[1] Embrapa Instrumentation (CNPDIA), P.O. Box 741, 13560-970, São Carlos, SP, Brazil
[2] Postgraduate Program in Computer Science, Federal University of São Carlos, São Carlos, SP, Brazil
Emails: bruno.moreno@estudante.ufscar.br; paulo.cruvinel@embrapa.br

***Abstract*—Smart farming has emerged as a new option to deal with the adversities of food generation in agriculture in the face of growing demand, with the aim of increasing productivity allied to the search for a more sustainable world. One of the objects of study in precision agriculture is weed control and the conscious use of inputs. This article presents the development and characterization of an embedded stereo system using camera sensors and Internet of Things principles, for future application in the area of digital image processing. Concepts of validation of lenses by Modular Transfer Function, calibration of intrinsic parameters of sensors and 3D system and memory and energy consumption management are analyzed, and implemented in the construction of an equipment, which aim to control invasive plants in crops.**

Keywords*—*camera sensor; stereo vision; embedded platform; weed control; agricultural industry.

I. Introduction

Agriculture is a very important source of food, feed, fiber and even fuel. Despite this, agriculture currently faces the challenge of increasing its production in response to the demand of continued population growth, taking precautions against the various adversities caused by the climate and minimizing the impact of man on nature [1].

One of the approaches aimed at increasing productivity in the field is the reduction of losses due to factors exogenous to crops, such as competition resulting from the presence of invasive plants. The presence of weeds in the cultivation area can decrease crop yield by more than 50% just by competing with the moisture present in the soil, causing more damage than invasive animals, diseases and other pests [2]. Therefore, weed control is essential so that the nutrients present in the soil, the development space and the reception of sunlight remain exclusively for the plant of interest [3].

Moreno and Cruvinel presented previous studies related to a stereo camera's system [4], and the development of a software based on semantic computing concepts for the segmentation of weed plants [5].

Although the use of pesticides has already been established to deal with this problem, technological applications aimed at the rational use of inputs are desired. Among such technologies, Computer Vision stands out, which works in two stages: image acquisition and image processing. The acquisition is made exclusively from camera sensors, capturing the environment and patterns present in digital images. Such sensors can then capture the visible or thermal spectrum, and be coupled to vehicles, devices, robots, drones and even satellites. On the other hand, affordable single-board computers have made onboard image processing possible [6].

Image processing can be summarized in five steps. In the first, the raw data are pre-processed, removing noise and selecting only the object of interest. In another step, pattern features are extracted, whereas in the case of plant images, such parameters are related to color, shape and texture. In the third stage, the features go through a selection process, decreasing the dimensionality of the data. Afterwards, the data are classified, grouping them based on their similarities. Finally, in the decision making stage, new input data can be classified from the already trained model, thus identifying which group it belongs to [7][8].

To ensure that the input data are of good quality, validating and using good camera sensors have become extremely important. Allied to this, other points of consideration in the application of such techniques in agriculture are the management of the volume of data generated, the data analysis techniques that need to deliver interpretable and understandable results due to the interdisciplinarity of workers in the area, and the mobile systems that need to be able of handle scarce resources such as limited battery life, low computational power and limited bandwidths for data transfer [9].

As examples of the use of camera sensors in the field, there are applications coupled to vehicles to operate during preplanting and analyze the height and density of vegetation from the images [10] and identify the location of invasive plants for manual control via weeding machine [11]. Plant images can also be acquired to create a database on an external server for further processing, for training a future classifier [12].

This paper is structured as follows. Section II presents the materials and methods used, including the Internet of Things (IoT) system description, camera sensor specifications, stereo vision basics, and embedded board specifications. Section III presents the results of the validation of the sensor and of the stereo system, the power supply and memory limitations and the final prototype, with the final conclusions in Section IV.

II. Materials and Methods

The developed system aims to capture stereoscopic images in a real environment of plantations, so that the presence and concentration of weeds present in the region of interest can be identified from an embedded algorithm. The capture of stereo images requires two camera sensors, generating two images of the same area that will be the input of the system. The images are then processed and grouped into classes, and the data will

 ISBN: 978-1-68558-083-4

be prepared for sending to a module external to the system, which will be responsible for spraying the site.

A. High-level IoT architecture

Embedded systems have a potential in agricultural use due to their mobility, low cost and computational power, allowing the performance of complex tasks in a more practical way. Raspberry Pi (RPi) is being used in several applications and it is the leading candidate for hardware implementation due to its powerful processor, rich I/O interface and compatibility that allows most projects to run on it [13]. Its wireless communication also makes the RPi capable of working with IoT projects, allowing objects to be sensed or controlled remotely across existing network infrastructure and reducing human intervention [14].

IoT systems in agriculture are separated into three modules: farm side, server side and client side. The farm side usually consists of detecting local agricultural parameters, identifying the location and sensor data, transferring crop fields data for decision making, decision support and early risk analysis based on recent data, and action and control based on the monitoring of the crop [15]. As can be seen from the block diagram in Figure 1, the developed IoT Stereo System can gather image data in the field, pre-process, segment, create feature extraction and depth information vector, classificate and interpret the collected data, while being controlled and monitored via Bluetooth serial communication by a mobile app.

On the server side, the network layer is responsible for reliable transformation to the application layer. A Wireless Personal Area Networks (WPAN) network can be mounted on a single board computer, with its own unified control and monitoring console for various wireless networks. Data transport and storage become essential, with data that can be saved on an external server or in the cloud, and then transferred to other devices, including the equipment responsible for product spraying on the plantation. The last module, the client side or application layer, collects and processes information, providing an environment where users can monitor data processed by the system via a web browser, anywhere and anytime.

B. Embedded System and Camera Sensor Specifications

RPi is a series of mini-embedded computers developed in the United Kingdom by the Raspberry Pi Foundation in association with Broadcom. The model used was the RPi 3 B+, where its specifications can be seen in Table I. It is important to note that board must be powered with a nominal voltage of 5 V capable of delivering 2.5 A of current, with operating temperature between 0 °C and 50 °C. The internal memory is defined from a micro Secure Digital (SD) card, where the kernel of the operating system is also present, being recommended the use of at least 8 GB of memory. The RPi 3 B+, unlike previous family models, enables BCM43438 wireless Local Area Network (LAN) and Bluetooth Low Energy (BLE) communication, allowing wireless data exchange.

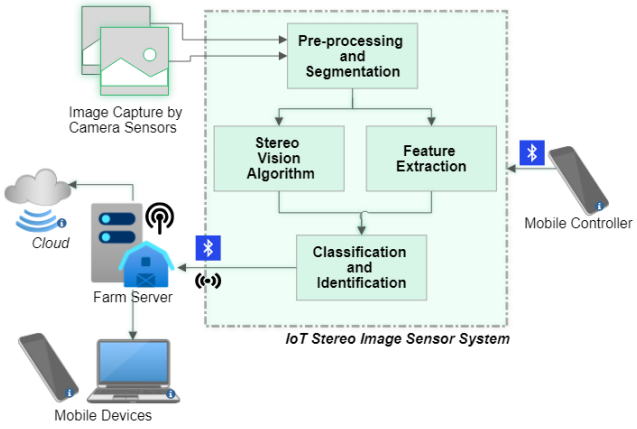

Figure 1. High-level system architecture diagram.

TABLE I
RASPBERRY PI 3 MODEL B+ CHARACTERISTICS

Processor	BCM2837B0 Cortex-A53 (ARMv8) 64-bit		
Clock	1.4 GHz	GPIO	40 pins
Memory	1 GB SDRAM	Gigabit Ethernet	1 connector
USB Port	4 USB 2.0	HDMI	1 connector
Camera serial interface (CSI)		Display serial interface (DSI)	
Wireless (dual band)		Bluetooth 4.2/BLE	
3,5mm 4 Jack output		Micro SD card slot	
Support Power-over-Ethernet		Input DC 5V/2.5A	

TABLE II
PI CAMERA CHARACTERISTICS

Size	25 x 24 x 9 mm
Resolution	5 MP
Video modules	1080p30, 720p60, 640x480p60/90
Sensor	OmniVision OV5647
Sensor resolution	2592 x 1944 pixels
Sensor image area	3.76 x 2.74 mm
Pixel size	1.4 μm x 1.4 μm
Optical size	1/4”
Full-frame SLR equivalent	35 mm
S/N Ratio	36 dB
Dynamic range	67 dB @ 8 times gain
Fixed focus	1 m - ∞
Focal length	3.60 ± 0.01 mm
Horizontal field of view (HFOV)	53.50° ± 0.13°
Vertical field of view (VFOV)	41.41° ± 0.11°
Focal ratio (F-stop)	2.9

The RPi has its own camera sensor alternatives, including the Pi Camera v1, with specs shown in Table II. Among the most important parameters, stand out the fixed focal length of 3.60 mm, the maximum sensor resolution of 2592 x 1944 pixels, and the camera opening angle of 53.50º horizontally and 41.41º vertically.

C. Modular Transfer Function as Camera Sensor Validation

The Modular Transfer Function (MTF) expresses how well an optical system preserves the contrast of spatial frequencies of the object in the image and is a well-established performance method [16]. A popular way to estimate the MTF curve for spatial frequency is called the inclined knife-edge method, in which the curve is obtained from a region of the image where there is a transition from a very dark tone to a very light

 ISBN: 978-1-68558-083-4

tone [17]. An Edge Spread Function (ESF) is calculated from the recorded knife edge, giving the one-direction response of the imaging system to an edge object. The Line Spread Function (LSF) is obtained by the derivative of the ESF.

Then, the use of a camera sensor can be defined taking into account the calculation of the LSF of the camera lens and MTF, which represents the magnitude response of the optical system to sinusoids of different spatial frequencies, i.e., retrieved by Fourier transform of the LSF. Taking a linear source the solution to measure the MTF is in 1D, orthogonally to the direction of the line. This can be proven considering a given source $S(x, y) = \delta(x).C$, and a lens of diameter equal to a, that means:

$$R(k_x, k_y) = \int \int_{-a/2}^{a/2} \delta(x) C e^{j(k_x x + k_y y)} dx dy \qquad (1)$$

The response of the objective can be expressed as the square of the Fourier transform of the product of the source with the aperture of the lens $R^2(k_x, k_y)$, with (k_x, k_y) the spatial frequencies associated with the spatial coordinator (x, y). Besides, looking for a solution of (1) and solving the integral by parts is possible to reach:

$$R^2(k_x, k_y) \alpha \frac{sin^2(ak_y)}{(ak_y)^2} \qquad (2)$$

Equation (2) corresponds to the LSF. The Fourier Transform of the LSF then gives the 1D MTF in the yy-direction. In stereo systems, usually the MTF system data are summarized as a curve for each sensor or just the curve of the lowest quality sensor [18]. Therefore, the images from the cameras are convolved based on the multiplication of their MTFs in the frequency domain.

D. Stereo Vision Principles

Stereo vision systems are usually based on the use of two cameras with the aim of simulating the human vision system and obtaining depth of objects, with the camera plane as a reference. The depth is acquired through the comparison of the object's position between each captured image [19]. The simplest way of comparing both images is guaranteed when the cameras are coplanar and aligned, as shown in Figure 2. The variables defined by the camera system are the baseline b and the focal distance f. The $P(X, Y, Z)$ represents a point that would be recorded by the two cameras and $u_L = (X_L, Y_L)$ and $u_R = (X_R, Y_R)$ are the projections of this point in each image. From the concepts of geometry and similarity of triangles, it is possible to obtain:

$$Z = \frac{bf}{X_L - X_R} = \frac{bf}{d} \qquad (3)$$

The d variable is called disparity. Thus, with two images as inputs in a calibrated and synchronized stereo architecture, depth information is obtained by finding the corresponding pixels in both images (u_L and u_R) by a matching algorithm and subtracting their X-axis coordinates. By performing this operation for all paired pixels in the image, the disparity map

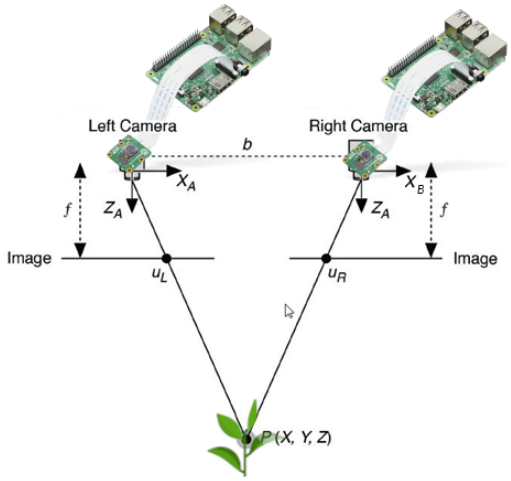

Figure 2. Stereo vision model.

is obtained, which contains all the depth information in the image.

It is also important to note the distortion that variations in the disparity map can cause in the depth estimation, i.e., verify the measurement obtained accuracy. So, for a variation in depth, it is possible to find:

$$\Delta Z = Z - \frac{bf}{d + \Delta d} = \frac{Z^2 \Delta d}{bf + Z\Delta d} \approx \frac{Z^2 \Delta d}{bf} \qquad (4)$$

During image capture, the focal length f and baseline b are fixed, but the baseline distance can be adjusted to minimize this distortion, taking into account the expected distance of objects from the camera. Thereby, the system calibration can be done from an image of a chessboard on which its pattern allows to rotate and adjust the stereo images so that they are lined up and the difference between them is only in the horizontal dimension. Before calibrating the system, it is necessary to find the calibration of each camera, which is defined by two matrices, the camera matrix and the distortion matrix [20]–[22]. The camera matrix, presented in (5), is composed of intrinsic parameters as focal length f_x and f_y, and optical centers c_x and c_y. On the other hand, (6) shows the distortion matrix, where q_1, q_2 and q_3 represent the lens radial distortion coefficients and p_1 and p_2 the lens tangential distortion coefficients.

$$camera\ matrix = \begin{bmatrix} f_x & 0 & c_x \\ 0 & f_y & c_y \\ 0 & 0 & 1 \end{bmatrix} \qquad (5)$$

$$distortion\ coefficients = \begin{bmatrix} q_1 & q_2 & p_1 & p_2 & q_3 \end{bmatrix} \qquad (6)$$

Finally, the calibration of the entire stereo vision system can be summarized by (7), where $\mathbf{R_x}$ represents the rotation factor and $\mathbf{T_x}$ the translation factor between the captured left and right image [23][24].

$$Left\ Image = \mathbf{R_x} * Right\ Image + \mathbf{T_x} \qquad (7)$$

Note that unlike the camera matrix and distortion coefficients which depend only on the camera, the $\mathbf{R_x}$ and $\mathbf{T_x}$ matrices must be recalculated if any stereo system settings change such as, for example, the baseline distance.

III. Results and Discussions

Experimental results were focused on the instrumentation' s characterization, i.e., including both the sensors and hardwares associated with signal and image processing. So far, the images for such a characterization were collected at laboratory level only. The system is based on eight elements, as follows: 12 V battery; 12 Vdc to 220 Vac voltage inverter; Light Emitting Diode (LED) lamp; 110-220 Vac to 5 Vdc rectifier; two RPis and two Camera Pi, as the schematic presented in Figure 3. All components are fixed on a metallic structure, with adjustable distance between cameras, angle of inclination (0º, 90º, 180º, 270º) and height of the cameras in relation to the ground (10 to 100 cm). The built system can be seen in Figure 4.

The system is controlled by an Android App via Bluetooth serial communication, where commands can be sent: synchronous image capture on the two RPis, send the images to the cell phone to check the quality of the capture, check the amount of images saved on memory, and board reboot or shutdown command. The RPis also communicate with each other via Bluetooth protocol, that supports up to 7 accessory devices, and uses Radio Frequency Communication (RFCOMM) Bluetooth protocol in data transfer with the cell phone. To ensure system security, it connects only to trusted equipment on specific ports.

A. Energy consumption management

A RPi can has power consumption of up to 12.5 W, but in laboratory tests the usual value during the application of the image capture software was only 3 W. As the system was designed with a inverter, the power consumed by this equipment must also be considered for system evaluation and possible improvements. In this case, the inverter in question presented a spent power of around 8.4 W, significantly higher than the sum of the RPis. To deal with such power, a battery of 12 V and 60 Ah was chosen.

To measure the energy expenditure of the system, current and power were calculated in different situations, according to Table III, with battery voltage fixed at 12.0 V. To evaluate the battery capacity, a test was carried out in the most extreme situation, with the system in continuous operation with the 18 W LED lamp on, which resulted in the maintenance of operation for approximately 15 hours. When the battery was discharged to 11.7 V, the inverter stopped as a safety precaution. It was observed that, in this operating mode, the peak current at system startup was close to 3.2 A, while with the same configuration but with the less potent LED lamp the peak was 2.0 A.

B. Memory management

For each RPi a 32 GB SD memory card was selected. After the initial settings, the necessary programs installed and the capture algorithm developed, about 23.1 GB of memory was free for general use. To ensure that the program can handle the amount of data written and stored, it is good to know how long the embedded system takes to save files. In testing, it was found that the SD card sequential memory write rate is 14833 KB/s or 14.8 MB/s.

Such information is important to define the resolution in which the images will be captured, as they define the size of the files saved in memory. Following the dimension of the camera sensor, it is preferable to define the resolution of the captured images to take advantage of the entire sensor size, that is, in which the 4:3 ratio is preserved. The maximum file size can be calculated by multiplying the resolution by the pixel depth, but since the Pi Camera doesn't have the option to format a RAW image file, the images are compressed, resulting in smaller files. So, it was tested five resolutions, 640 x 480, 800 x 600, 1024 x 768, 1280 x 960 and the maximum 2592 x 1944. Early test results can be seen on Figure 5, where five images in each resolution were taken and saved in the PNG format.

Considering the future application in image processing, in which the computational cost of operations tends to grow

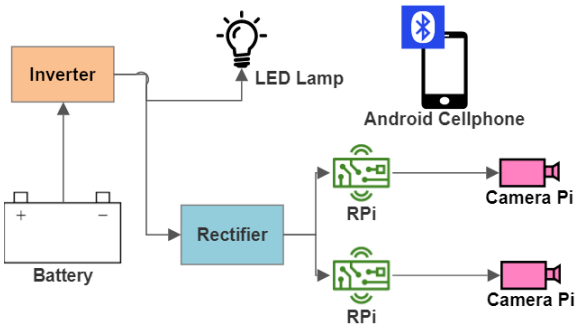

Figure 3. Diagram of the connection between the components.

(a) Details of the camera, stereo rig and lamp.

(b) Interior of protective case, with RPis and rectifier.

Figure 4. Developed system.

TABLE III
System Power At Different Settings

Mode of operation	Current (A)	Power (W)
Standard	1.3	15.6
With active camera sensors	1.4	16.8
With active camera sensors and 4.5 W LED lamp	1.9	22.8
With active camera sensors and 18 W LED lamp	3.0	36

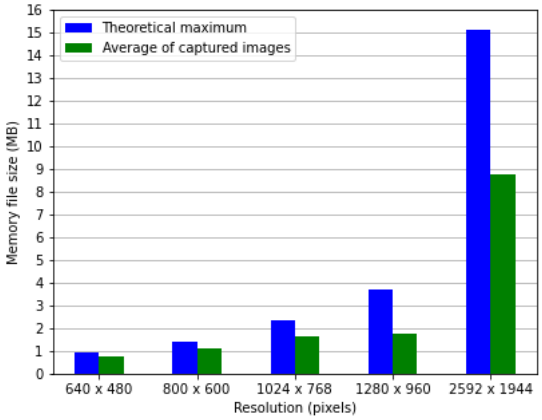

Figure 5. Image file size experimentations.

(a) Left Camera. (b) Right camera.

Figure 6. Images of a calibration chessboard, captured synchronously and without being processed.

exponentially according to the number of pixels present, and the available SD memory, the resolution of 1280 x 960 was then chosen. With this resolution, at least 6,000 images can be saved in memory, although it is possible to store them later in the cloud, from the system's communication with an external network, freeing up space on the board. It should be noted that for future applications, if the maximum resolution is used, the memory writing time must be taken into account as a limiting factor.

C. Camera sensor validation

The first step in calculating the stereo MTF was to capture an image of the chessboard with both cameras at the same time, as can be seen in Figure 6. For each image, five random regions were selected where there are knife edges recorded, in the same location for both cameras. The normalized MTF was calculated for each point and averaged between them, and after that, the MTF of the stereo system was then calculated from the multiplication of both MTFs, as can be seen in Figure 7. The MTF value at the Nyquist frequency was then 14.31% for the left camera, 8.97% for the right and 1.28% for the entire system.

To evaluate the camera's SNR ratio, only the regions of the converted grayscale image where black blocks were presented, which have a uniform color on the original chessboard, were used, and the mean and standard variation of the signal were evaluated. For the right camera, the calculated value was

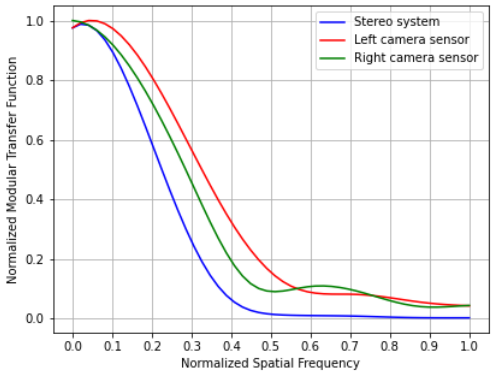

Figure 7. MTF of each camera sensor and combined system.

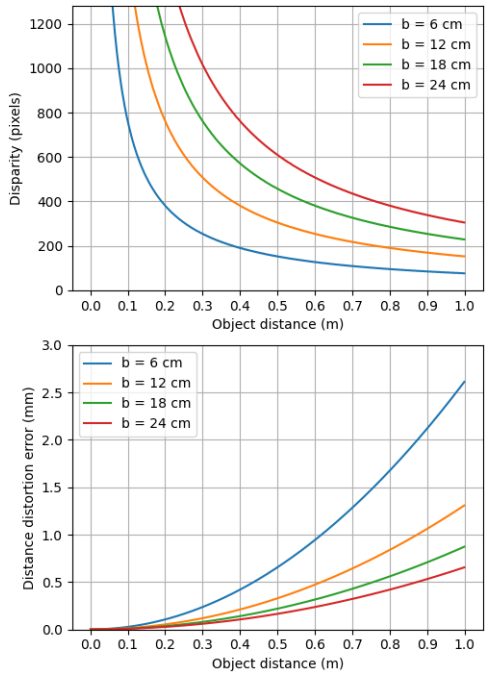

Figure 8. Baseline distance disparity and distortion error evaluation.

19.7 dB, while for the left camera it was 17.9 dB, below the 36 dB specified by the manufacturer.

D. Stereo vision parameters

The first step in tuning the stereo system is to define the baseline distance that will be used to capture the images. The developed prototype has a minimum possible baseline of 6 cm and a maximum of 24 cm, which makes it capable of simulating human vision, which has this value in the range of 5.4 to 7.4 cm, in addition to allowing the exploration of other scenarios. For this, considering (3) and (4), the expected disparity for an object up to 1 m away from the camera and the expected distortion error at such distance were calculated, for four values of baseline, 6 cm, 12 cm, 18 cm and 24 cm, as can be seen in the Figure 8, considering the resolution of 1280 x 960.

 ISBN: 978-1-68558-083-4

When setting the baseline distance, it is always preferable to use the lower values to ensure greater interpolation between the two generated images, which allows closer objects to have their distance calculated. For example, according to the graph shown, for b = 24 cm, objects up to 23.8 cm away from the camera would not be present in both images, making it impossible to calculate the disparity, while for b = 6 cm such a situation is only valid for objects less than 5.9 cm away. As for objects of up to 1 m, the distortion error proved to be small for all cases, including for the scenario with the smallest baseline, so it can be defined that the best use of the stereo system occurs for values close to 6 cm.

Thus, for b = 6 cm and height of 1 m (value chosen so that, due to the height of the growing plants, the object under analysis is not too close to the sensors), the calibrated parameters results of the left and right cameras, and of the stereo system, were:

$$\textit{Left camera matrix} = \begin{bmatrix} 736 & 0 & 582 \\ 0 & 735 & 464 \\ 0 & 0 & 1 \end{bmatrix} \tag{8}$$

$$\textit{Left distortion coefficients} = \begin{bmatrix} 0.0589 \\ -0.169 \\ 0.00139 \\ 0.00198 \\ 0.142 \end{bmatrix}^{\mathsf{T}} \tag{9}$$

$$\textit{Right camera matrix} = \begin{bmatrix} 1480 & 0 & 681 \\ 0 & 1480 & 480 \\ 0 & 0 & 1 \end{bmatrix} \tag{10}$$

$$\textit{Right distortion coefficients} = \begin{bmatrix} -0.0728 \\ 3.98 \\ 0.00117 \\ 0.00630 \\ -22.6 \end{bmatrix}^{\mathsf{T}} \tag{11}$$

$$\mathbf{R_x} = \begin{bmatrix} 0.960 & -0.0133 & -0.281 \\ 0.0159 & 1.00 & 0.00721 \\ 0.280 & -0.0114 & 0.960 \end{bmatrix} \tag{12}$$

$$\mathbf{T_x} = \begin{bmatrix} -0.787 \\ -0.0670 \\ 5.65 \end{bmatrix} \tag{13}$$

Note that if the baseline distance is changed, it is necessary to calibrate the system again, recalculating only the $\mathbf{R_x}$ and $\mathbf{T_x}$ matrices, but it is expected that $\mathbf{R_x}$ will not change significantly, as the mounted structure does not allow the cameras to yaw, pitch or roll.

IV. Conclusion and Future Work

The results showed a characterization process of an IoT stereo image sensor system, capable of capturing and transferring validated images via wireless commands, ready to be used in real agricultural field conditions. Such developed embedded vision system can be useful for applications in 3D image processing, with several variable parameters that allow the adaptation of the system to different situations, although the power supply can be simplified to reduce the weight and power spent of the system, allowing the use of smaller batteries and fewer components (for example, with only a 12 Vdc to 5 Vdc converter and 9 W 12 V LED lamp).

For future steps, it is desired to carry out agricultural analyzes, considering weed families, as well as the inclusion of AI-based weed image process to identify plant species for agricultural control. In addition, an expansion of system's connectivity with other devices will also be realized.

Acknowledgment

This work has been supported by Embrapa and Brazilian research agency CAPES.

References

[1] FAO, "The future of food and agriculture – alternative pathways to 2050," Food and Agriculture Organization of the United Nations Rome, pp. 224, 2018.

[2] H. Abouziena and W. Haggag, "Weed control in clean agriculture: a review," Planta daninha, SciELO Brasil, vol. 34, pp. 377–-392, 2016.

[3] S. C. Bhatla and M. A. Lal, "Plant physiology, development and metabolism," Springer, 2018.

[4] B. M. Moreno and P. E. Cruvinel, "Sensors-based stereo image system for precision control of weed in the agricultural industry," SENSORDEVICES 2018, The Ninth International Conference on Sensor Device Technologies and Applications, pp. 69–76, 2018.

[5] B. M. Moreno and P. E. Cruvinel, "Computer vision system for identifying on farming weed species," 2022 IEEE 16th International Conference on Semantic Computing (ICSC), USA, pp. 287–292, 2022.

[6] M. I. Sadiq, S. M. P. Rahman, S. Kayes, A. H. Sumaita, and N. A. Chisty, "A review on the imaging approaches in agriculture with crop and soil sensing methodologies," 2021 Fifth International Conference On Intelligent Computing in Data Sciences (ICDS), Morocco, pp. 1–7, 2021.

[7] M. Rajoriya and T. Usha, "Pattern recognition in agricultural areas," Journal of Critical Reviews, vol. 7, pp. 1123–1127, 2020.

[8] J. Wäldchen, M. Rzanny, M. Seeland, and P. Mäder, "Automated plant species identification—trends and future directions," PLoS computational biology, vol. 14, pp. 1–19, 2018.

[9] M. P. Raj, P. R. Swaminarayan, J. R. Saini, and D. K. Parmar, "Applications of pattern recognition algorithms in agriculture: a review," International Journal of Advanced Networking and Applications, vol. 6, pp. 2495–2502, 2015.

[10] D. Mcloughlin, "Image processing apparatus for analysis of vegetation for weed control by identifying types of weeds," EP1000540, May 17, 2000.

[11] J. Gao and Z. Jin, "Bionic four-foot walking intelligent rotary tillage weeding device, has weeding system installed on back side of machine body, where gear in gear rotating mechanism transmits power to rotary shaft that is provided with weeding cutter," CN114794067, Jul 29, 2022.

[12] X. Jin, Y. Chen, and J. Yu, "Precise weeding method for lawn and pasture based on cloud-killing spectrum, involves receiving images uploaded by each weeding robot, completing weed identification and outputting spraying instructions, and collecting and organizing massive weed data for big data applications," CN113349188, Sep 7, 2021.

[13] S. E. Mathe, M. Bandaru, H. K. Kondaveeti, S. Vappangi, and G. S. Rao, "A survey of agriculture applications utilizing raspberry pi," 2022 International Conference on Innovative Trends in Information Technology (ICITIIT), Kottayam, India, pp. 1–7, 2022.

[14] C. Balamurugan and R. Satheesh, "Development of raspberry pi and IoT based monitoring and controlling devices for agriculture," pp. 207–215, 2017.

[15] K. A. Patil and N. R. Kale, "A model for smart agriculture using IoT," 2016 International Conference on Global Trends in Signal Processing, Information Computing and Communication (ICGTSPICC), Jalgaon, India, pp. 543–545, 2016.

 ISBN: 978-1-68558-083-4

[16] O. van Zwanenberg, S. Triantaphillidou, R. Jenkin, and A. Psarrou, "Edge detection techniques for quantifying spatial imaging system performance and image quality," in Proceedings of the IEEE/CVF Conference on Computer Vision and Pattern Recognition Workshops, pp. 1871–1879, 2019.

[17] N. Kawagishi, R. Kakinuma, and H. Yamamoto, "Aerial image resolution measurement based on the slanted knife edge method," in Optics Express Vol. 28, pp. 35518–35527, 2020.

[18] A. A. Naumov, A. V. Gorevoy, A. S. Machikhin, V. I. Batshev, and V. E. Pozha, "Estimating the quality of stereoscopic endoscopic systems," in Journal of Physics: Conference Series Vol. 1421, pp. 012044, 2019.

[19] L. Yang, B. Wang, R. Zhang, H. Zhou, and R. Wang, "Analysis on location accuracy for the binocular stereo vision system," in IEEE Photonics Journal, vol. 10, no. 1, pp. 1–16, Art no. 7800316, Feb. 2018.

[20] Y. M. Wang, Y. Li, and J. B. Zheng, "A camera calibration technique based on OpenCV," The 3rd International Conference on Information Sciences and Interaction Sciences, Chengdu, China, pp. 403–406, 2010.

[21] J. Sun, X. Chen, Z. Gong, Z. Liu, and Y. Zhao, "Accurate camera calibration with distortion models using sphere images," in Optics & Laser Technology, Vol. 65, pp. 83–87, 2015.

[22] J. Salvi, X. Armangué, and J. Batlle, "A comparative review of camera calibrating methods with accuracy evaluation," in Pattern Recognition, Vol.35, Issue 7, pp. 1617–1635, 2002.

[23] S. Yang, Y. Gao, Z. Liu, and G. Zhang, "A calibration method for binocular stereo vision sensor with short-baseline based on 3D flexible control field," in Optics and Lasers in Engineering, Vol. 124, pp. 105817, 2020.

[24] Y. Wang, X. Wang, Z. Wan, and J. Zhang, "A method for extrinsic parameter calibration of rotating binocular stereo vision using a single feature point," in Sensors, Vol. 18, Art no. 3666, pp. 1–16, 2018.

 ISBN: 978-1-68558-083-4